

Vladimir Pelmeshnikov · Margareta R.A. Blomberg
Per E.M. Siegbahn

A theoretical study of the mechanism for peptide hydrolysis by thermolysin

Received: 28 May 2001 / Accepted: 22 August 2001 / Published online: 27 September 2001
© SBIC 2001

Abstract The catalytic mechanism for peptide hydrolysis by thermolysin has been investigated using the B3LYP hybrid density functional method. The starting structure for the calculations was based on the X-ray crystal structure of the enzyme inhibited with the ZF^pLA phosphoramidate transition-state analogue. Besides the three Zn ligands His142, His146 and Glu166, a few additional residues were also included in the model. Following the order of importance, the outer-sphere ligands Glu143, His231 and Asp226 were shown to play significant catalytic roles, well correlated with results from site-directed mutagenesis experiments. A single-step reaction mechanism was obtained starting from the initial enzyme-substrate complex with a pentacoordinated metal center and proceeding to the enzyme-carboxylate complex as a final product, following a proposal by Matthews and co-workers. The transition state combines a nucleophilic water oxygen attack on the peptide carbon and a proton transfer from the water to the peptide nitrogen, mediated by the Glu143 carboxylate. A free activation energy of 15.2 kcal/mol was obtained, compared to the experimental 12.4–16.3 kcal/mol range for various peptide substrates. An interesting aspect of the present single-step mechanism is that the Glu143 carboxylate moves a significant distance of ~1.0 Å. Different chemical models were examined, both related to the system size and proper side-chain modeling. The significance of the protein frame rigidity around the active site was estimated by fixing and subsequently releasing the edge atom positions. Finally, alternative mechanistic proposals are briefly summarized.

Keywords Thermolysin · Peptide hydrolysis · Catalytic mechanism · Density functional theory

Introduction

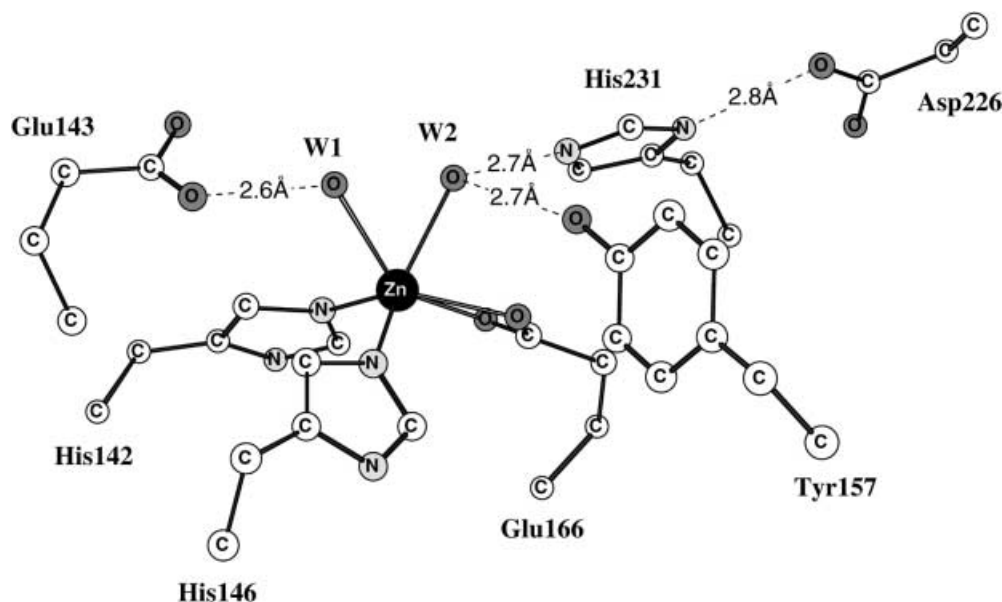
Zn²⁺-containing metalloproteases constitute an expanding list of structurally related proteases which are widely distributed in Nature. They are involved in biochemical events of extreme importance, such as digestion (carboxypeptidase A, astacin), tissue remodeling and extracellular matrix degradation (matrix metalloproteinases), blood-pressure regulation (neprilysin), formylation and deformylation in bacterial protein synthesis (peptide deformylases), etc. [1]. Recently, zinc peptidases have attracted increased attention as model proteins for structure-based drug design [2, 3], to be used for treatments of a number of diseases such as tumor invasion, arthritis and bone destruction.

Thermolysin (TLN, classification number EC 3.4.24.27) is a typical example from the Zn²⁺-metalloprotease superfamily. Isolated from *Bacillus thermoproteolyticus* [4], this extracellular endopeptidase catalyses hydrolysis of the peptide bond specifically on the imino side of large hydrophobic residues [5, 6], in particular leucine, isoleucine and phenylalanine. Besides a purely physiological activity, TLN has been found to be a useful catalyst in protein engineering [7] owing to its high thermostability and narrow substrate specificity. A few industrial applications are also available, such as for the synthesis of the artificial sweetener aspartame [8] and as inclusion in laundry detergents for removal of protein stains.

TLN is one of the most studied metalloenzymes and, for a number of free enzyme and inhibitor complexes, detailed X-ray structures have been obtained, the first one in 1972 in pioneering work by Matthews et al. [9, 10, 11]. These structures show that the active site of the wild-type TLN (see Fig. 1) has two histidines (His142, His146) and one glutamate (Glu166) residue coordinating a Zn cation. There is a distorted tetrahedral coordination of the metal binding site of TLN, where one position exposed to solvent water turns out to always be present for catalytic zinc metalloproteins [12, 13, 14, 15].

V. Pelmeshnikov · M.R.A. Blomberg · P.E.M. Siegbahn (✉)
Department of Physics, Stockholm Center for Physics,
Astronomy and Biotechnology (SCFAB),
Stockholm University, 106 91 Stockholm,
Sweden

Fig. 1 The thermolysin active site structure, generated from X-ray data [16]



In a more recent TLN structure analysis [16], water appears in two alternatively occupied positions W1 and W2. The Glu143 residue, which is positioned in the second coordination shell of the zinc cation, forms together with the above-mentioned two histidines the consensus HEXXH motif of the enzyme amino-acid sequence [1]. Though the overall sequence and backbone conformations of the related enzymes display very different binding modes, the zinc-binding HEXXH motif is highly conserved between all the members of the mononuclear zinc endoproteases family, thus implying evolutionary converged or inherited reaction mechanisms [1, 2]. The distance of 2.6 Å between the W1 oxygen and the carboxylate oxygen of Glu143 in the X-ray structure (resolved to 1.7 Å) suggests the presence of strong hydrogen bonding (see Fig. 1). To a lesser extent, the same conclusion also holds for His231 and Tyr157, which are within hydrogen-bonding distance of 2.7 Å from the second water W2 oxygen. Site-directed mutagenesis studies, which have been performed to assess the importance of most residues in the vicinity of the active site, show that Glu143 has a key role in catalysis. Glu143-substituted thermolysin-like proteases (TLPs) show no observable secretion [17, 18]. His231 and Tyr157 mutated thermolysins [17, 19, 20] recover their residual proteolytic activity with a reduction of the k_{cat} values, corresponding to an increase of the ΔG^\ddagger free activation energy of the enzyme-substrate complex by 3.4–3.7 and 2.7 kcal/mol, respectively. There are also a few more residues rather far from zinc, known to cause considerable decreases in TLN activity when they are mutated [21, 22]. The Asp226-targeted (Fig. 1) mutagenesis affects k_{cat} by a 4-fold decrease [20], equivalent to an ΔG^\ddagger increase of 0.8 kcal/mol.

Despite extensive crystallographic studies, site-directed mutagenesis and kinetic investigations accumulated for thermolysin and homologous enzymes over

the years, the reaction mechanism is still under debate. A widely circulated proposal, originating from Pangburn and Walsh in 1975 [23] and refined by Matthews and co-workers during 1977–1988 [24, 25, 26, 27, 28], has been generalized to the entire TLP class. Based on structural analysis of the enzyme-inhibitor complexes believed to model different stages of the catalytic pathway, this proposal incorporates the Glu143, His231, Tyr157 and Asp226 outer-shell residues mentioned above, and proceeds as shown in Fig. 2. Starting from the unligated TLN **1**, with a Zn-coordinated water molecule, the wide groove separating the enzyme in two large domains accommodates an extended peptide chain, forming the Michaelis complex **2**. The carbonyl oxygen of the scissile peptide becomes wedged between His231, Tyr157 and the water molecule in the proximity of the zinc cation. When this occurs, the water molecule is displaced towards Glu143 and undergoes a strong polarization between the negative carboxylate and the positive Zn^{2+} . The mutual influence of the glutamate and the metal ion strongly enhances the nucleophilicity of the water oxygen, promoting an attack on the carbonyl carbon. The proton accepted by Glu143 is immediately shuttled to the nitrogen. As a result, a tetrahedral *gem*-diolate intermediate **3** is formed, where zinc is pentacoordinated and the peptide carbon is tetrahedral. The evidence for the existence of the **3**-like structure with five-coordinated zinc comes from transition-state analogue inhibitors [1, 25, 26, 27, 28], including phosphoramidate ZF^pLA , the most potent inhibitor ever observed binding to TLN with K_i of 0.068 nM [29]. The formation of hydrogen bonds from the side chains of His231 and Tyr157 with the carbonyl oxygen facilitates the formation of **3**. The negative carboxylate motif of Asp226, linked to the protonated His231, helps to stabilize the positive charge required for catalysis, in agreement with Asp226-targeted mutagenesis (see above mentioned data for the k_{cat}

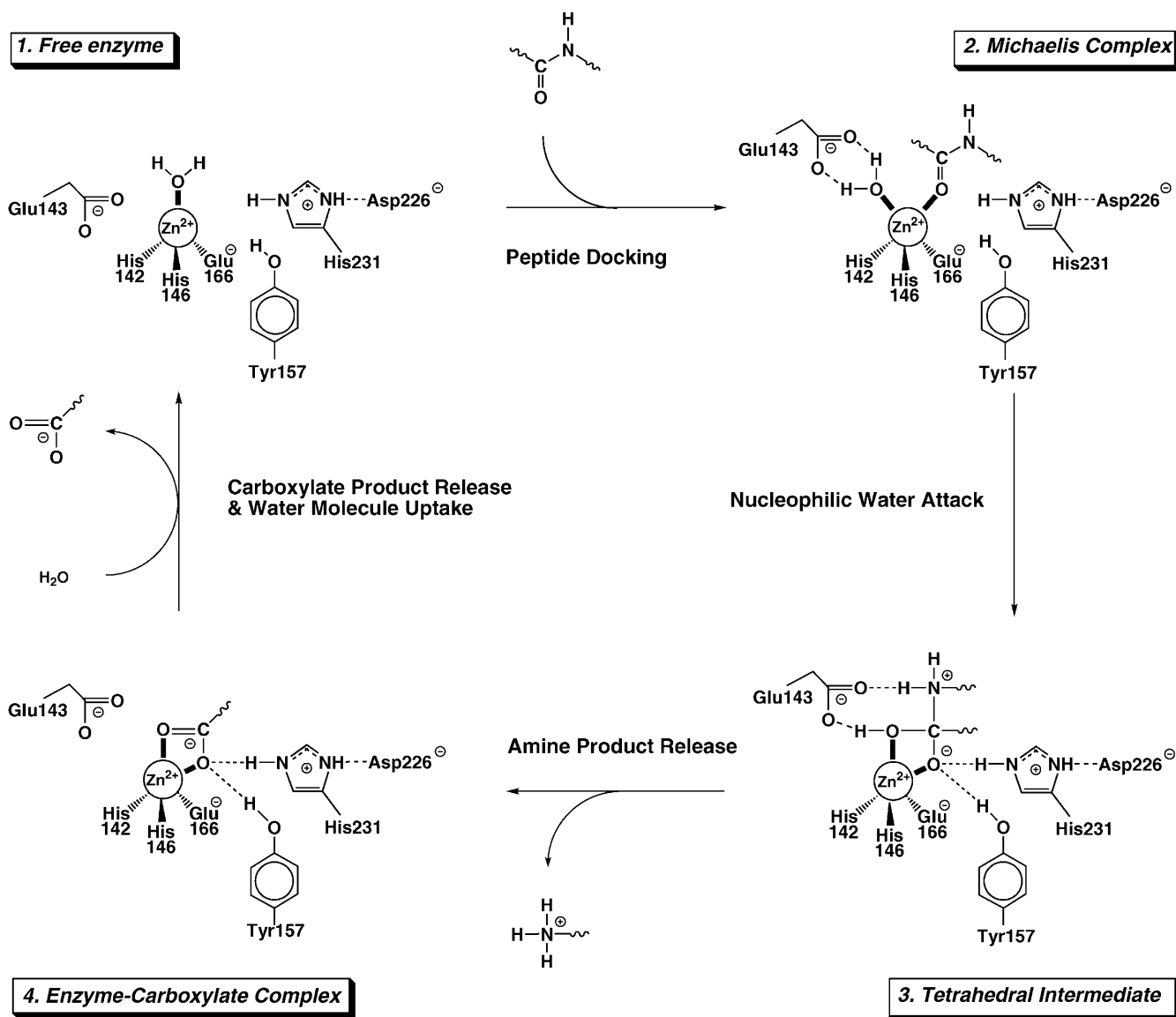


Fig. 2 Experimentally proposed reaction cycle for TLN [26, 28]

turnover number). In the next step, a direct cleavage of the peptide C-N bond takes place, with the amine product proposed to be released in its protonated form, fitting the neutral pH conditions. Again, Glu143 here serves as a proton shuttle, abstracting the second proton from the water oxygen and delivering this proton to the amine nitrogen. The catalytic cycle is closed by the carboxyl product detachment, probably mediated by the incoming water molecule uptake.

Recently, an alternative mechanism was suggested by Mock et al. [30, 31], based on the catalytic pH dependence of the Michaelis-Menten kinetic parameters for arazofornyl dipeptide substrates. In this mechanism, His231 acts as a general base in its neutral form, polarizing the attacking water molecule, similar to the role of Glu143 in Fig. 2. The latter residue is suggested to provide an electrostatic stabilization of the active site with its anionic side-chain, but in no other way to

participate in catalysis. The water molecule is proposed to leave its metal coordination upon the substrate carbonyl binding. The hydrolysis in this case has been shown to have the reverse protonation nature, i.e. the more acidic pH-dependent active unit (proposed to be the Zn-bound water) with the lower pK_a value of 5.16 is protonated and the less acidic one (the His231 residue) with the higher pK_a value of 8.26 is deprotonated in the active TLN form. This should result in the same bell-shaped profile of k_{cat}/K_m against pH as the protonation process described above, but the reverse protonation catalytic pathway appears to be less favored. First, the essential role of the His231 residue is not supported by mutagenesis studies (see above). Also, no His231 residue analogues are found in some of the Zn peptidases, believed to act in a high resemblance to TLPs. Furthermore, solely a charge stabilization role of Glu143 appears unlikely, since replacement of this Glu with Asp leads to totally inactive mutants, even though the Asp side-chain has the same negative charge [19]. The pK_a

values assigned to the Zn-bound water and the His231 residue are matters of discussion [1].

A few quantum chemical investigations of the TLN mechanism have been carried out by Rivail et al. [32, 33]. Single-point density functional calculations at the BLYP level in AM1-optimized geometries were performed for a quite simple model consisting of a formamide and adding one or two water molecules. The barrier for hydrolysis was computed to be 39.9 kcal/mol using one water and 18.5 kcal/mol using two water molecules [32]. In a second stage of modeling, QM/MM calculations were performed with the active site treated at the AM1 level and the surrounding protein at the MM level. Interestingly, inclusion of the surrounding protein resulted in a slight increase of the activation energy for hydrolysis. In a recent QM/MM study [33] the authors follow the mechanism by Matthews et al. [28]. Too high activation barriers (up to 41.6 kcal/mol) were obtained, however, probably owing to an overestimation of the energy barriers at the AM1 semiempirical level.

The above detailed information about the different steps and intermediates in the catalytic cycle of thermolysin, combined with the known X-ray structures, provide an ideal starting point for a quantum chemical study of the mechanism. The main goal of the present work is to investigate the most important catalytic aspects of the thermolysin reaction sequence, i.e. the cleavage of the peptide bond at the active site which occurs via a nucleophilic attack by water on the substrate carbon. Besides giving detailed energetics for the reaction steps, which can be used to test the suggested mechanism, the calculations provide additional information such as structures for short-lived intermediates and transition states. Also, the role of individual residues can be studied in detail as a complement to the picture provided by site-directed mutagenesis experiments. Besides the zinc-coordinating ligands His142, His146 and Glu166, the side-chains of the second shell residues Glu143, His231 and Asp226 are also included in different models, and their importance is estimated.

Materials and methods

Computational details

The B3LYP hybrid density functional method [34, 35, 36] as implemented in the GAUSSIAN-94 program package [37] was used for all the present calculations. For the geometry optimization, the LANL2DZ basis set was used. For the zinc atom this means the Los Alamos non-relativistic ECP by Hay and Wadt [38]. The valence shell, including the 3d orbitals, is described by a basis set of essentially double-zeta quality including a diffuse 3d-function. For the rest of the atoms, LANL2DZ implies the Dunning-Huzinaga full double-zeta basis set [39]. To achieve accurate energy values for the stationary points along the reaction pathway, single-point calculations for the B3LYP/LANL2DZ optimized geometries were carried out using an extended basis set. A single set of diffuse sp-functions were added on the heavy atoms and a set of polarization functions were added on all atoms. The extra functions were taken from the 6-311+G(1d,1p) triple-zeta basis set.

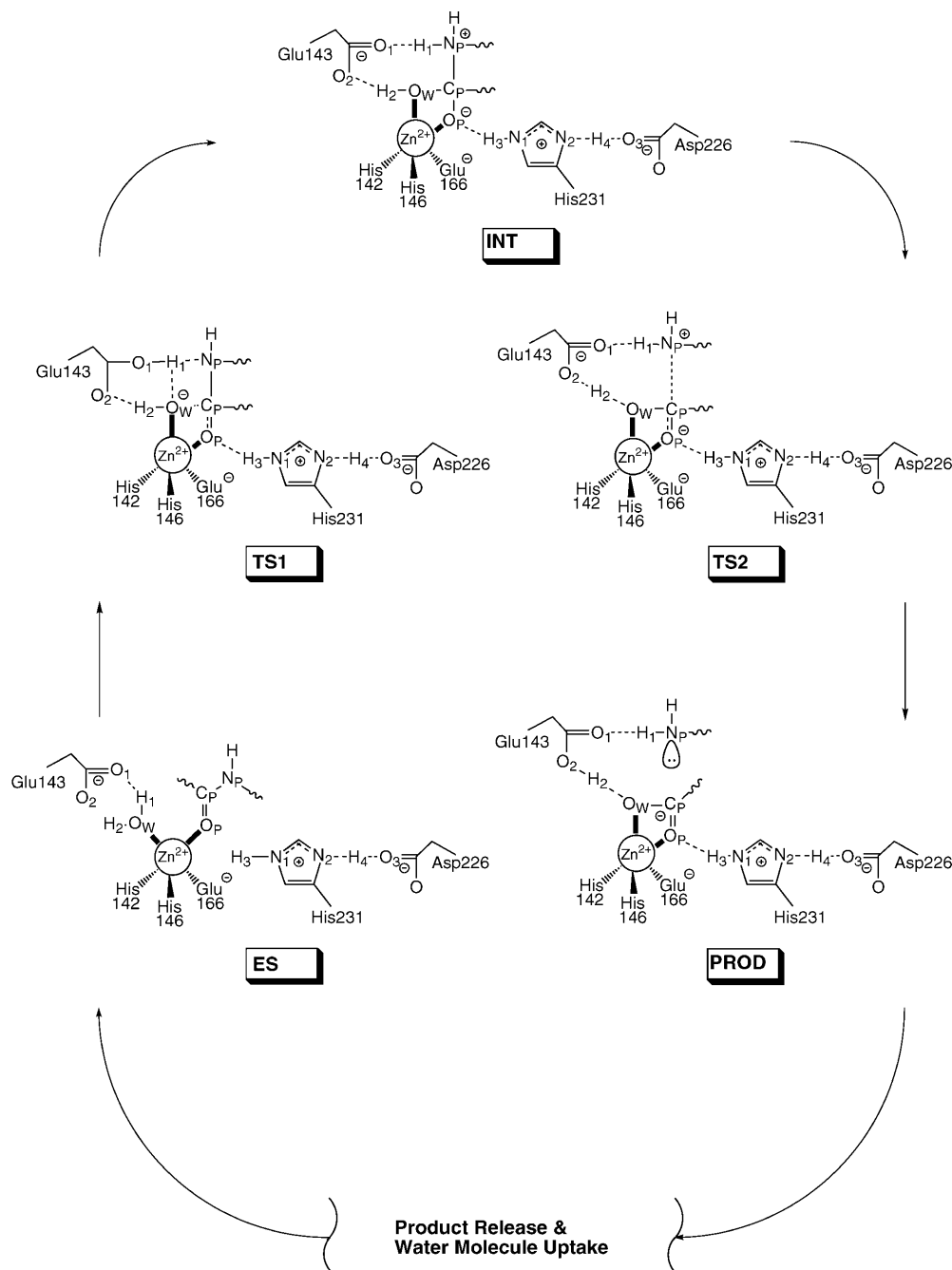
Each transition state located was characterized by calculating a Hessian matrix at the B3LYP/LANL2DZ level, verifying that it contains only one negative eigenvalue, with vibrational vectors leading to the desired neighboring minima. However, attempts to use intrinsic reaction coordinate (IRC) [40, 41] following schemes were unsuccessful owing to technical difficulties.

Zero-point thermal-corrected vibrational effects and entropy contributions [42] to the energy were obtained at 298.15 K, based on the computed Hessians. The zero-point corrections are within 0.9 kcal/mol for different stationary points. The relative entropy contributions are within 2.9 kcal/mol. The self-consistent isodensity polarized continuum model (SCI-PCM) [43, 44], as implemented in GAUSSIAN-94, was used in order to estimate the effects of the protein environment. The cavity containing the molecular system of interest is defined self-consistently by the surface with the default isodensity value of $0.0004e/B^3$, which has been shown to yield volumes close to the measured molar ones. The dielectric constant was chosen equal to 4, as commonly used for proteins [45]. The solvation effects were calculated for the geometries of the B3LYP/LANL2DZ optimization. According to several proposals, electrostatic interactions might play an active role in the course of peptide cleavage by TLN [26, 46, 47], supported by the presence of the formal charges on the chemical units of the active site and charge redistribution during the reaction. However, all these residues at the active site are included in the quantum chemical model, and the SCI-PCM approach therefore only gives rather negligible relative effects of about 1 kcal/mol.

Results and discussion

In the present study, several models for the TLN active site were investigated, mostly following the mechanistic approach as shown in Fig. 3 and based on the proposal by Matthews et al. [28] as in Fig. 2. Other mechanisms were also tried. Total charge neutrality and a singlet spin state are conserved among all the different models discussed in this section. The free energies presented below are based on the extended basis set results in the B3LYP/LANL2DZ optimized geometries, and include dielectric effects as described in the ‘‘Computational details’’ section, if not otherwise mentioned. The differences between the models used are related both to the size of the system and to the level of theory chosen. The models are briefly described in Table 1. In the largest model (C), which contains 68 atoms, the histidines are represented by their imidazole side-chains while the aspartate and glutamates are modeled by their carboxylate side-chains and with a varying number of atoms modeling its connection to the peptide backbone. The largest model is used for the Glu143 residue, which is modeled by a butyrate group. A characteristic feature of the models used is that an atom of each residue is locked into its position in the X-ray structure of the inhibited enzyme [27]. These atoms are marked in the figures below. In the case when this atom is a model hydrogen atom, its position was locked at a distance of 1.10 Å away from the carbon of the side-chain in the X-ray structure. The reason for applying these constraints in the geometry optimization is that especially the second-shell residues tend to wander rather far away from their original positions, which would not happen in the enzyme. The effects of releasing the constraints imposed by freezing

Fig. 3 The main mechanism investigated for the peptide bond cleavage by TLN. Strong hydrogen bonds and bond rearrangements in the transition states are given by *dashed lines*. Charges given are the formal ones



certain atoms in the present models were tested at the end of the study, which should give an estimate of the importance of the possible hinge-bending motions [16, 22, 48] for the catalysis, and these results are discussed below. The substrate, modeled by *N*-methylacetamide in the largest model, was left without any constraint in the optimization.

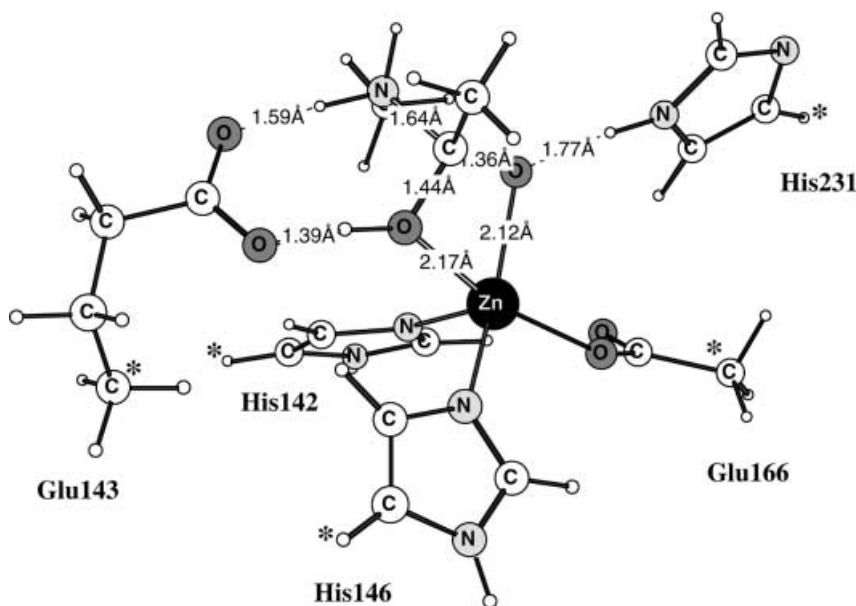
The *gem*-diolate intermediate

The natural starting structure for the present study of the TLN mechanism is the enzyme-inhibitor complex

with ZF^PLA, mentioned above. Believed to mimic the midpoint on the catalytic pathway (3-like structure in Fig. 2), the inhibitor contains tetrahedral phosphonamide phosphorus, mimicking the *gem*-diolate sp³ carbon. The coordinates were extracted from the PDB file 4TMN resolved to 1.7 Å [27] and phosphorus was replaced by carbon. As suggested by the internuclear separations between the Glu143 oxygens and ZF^PLA atoms found in 4TMN, corresponding to O_W-O₂=2.3 Å and N_P-O₁=3.3 Å in our system (notations are as used in Fig. 3), these linkages were protonated with H₂ and H₁, respectively. Similarly, the O_P-N₁=2.7 Å linkage was protonated with H₃. The model

Table 1 Different models for the substrate and active-site amino acid residues used for the reaction study

Model	Size, atoms	Substrate	Glu143	His231	His142, 146	Glu166	Asp226
A	63	<i>N</i> -Methylacetamide	Butyrate	Imidazole	Imidazole	Acetate	–
A'	43	<i>N</i> -Methylacetamide	Formate	Imidazole	Imine	Formate	–
A ⁺	44	<i>N</i> -Methylacetamide	Formate	Imidazolium	Imine	Formate	–
B	54	<i>N</i> -Methylacetamide	Butyrate	–	Imidazole	Acetate	–
C	68	<i>N</i> -Methylacetamide	Butyrate	Imidazole	Imidazole	Acetate	Formate
C'	45	<i>N</i> -Methylformamide	Formate	Imidazole	Imine	Formate	Formate
D ⁺	40	<i>N</i> -Methylformamide	Formic acid	–	Imidazole	Formate	–
E	46	<i>N</i> -Methylacetamide	Butyrate	–	Imine	Formate	–

Fig. 4 Optimized *gem*-diolate intermediate INT structure. Atoms marked with an asterisk were frozen during the optimization

used for the optimization of the *gem*-diolate intermediate is model A in Table 1 and contains 63 atoms. The optimized structure including key distances is shown in Fig. 4 (corresponds to INT in Fig. 3). A very close match with the starting inhibited TLN geometry was obtained. Superimposed structures are shown in Fig. 5, and a few important geometrical parameters are given in Table 2.

As can be seen from Fig. 4, the O_W-H_1 bond of the water molecule is already cleaved in the INT structure and both the proton and the hydroxyl group are bound to the activated substrate. Stabilization of this complex is provided by all the surrounding distinct units of the enzyme, in good agreement with the crystallography-based analysis of the inhibited TLN structure by Matthews et al. [26, 28]. The zinc cation coordinates the negative *gem*-diolate in a bidentate fashion, His231 forms a hydrogen bond to the peptide oxygen, and Glu143 perfectly binds the hydrated peptide with the oxygens O_1 and O_2 of the carboxylate group, forming two hydrogen bonds. The distances between the heavy atoms (in Table 2) indicate that there is a strong interaction in these latter hydrogen bonds, especially for the pair O_W-O_2 with a bond distance of only 2.45 Å.

Initial enzyme-substrate complex and the nucleophilic attack by water

In order to locate transition states and intermediates in the TLN mechanism as in Fig. 3, the tetrahedral intermediate INT complex was used as a starting point for searching backwards and forwards along the reaction profile. This was done by stepwise constraining certain geometrical parameters. Scanning backwards, the initial enzyme-substrate complex ES and the transition state TS1 were eventually found.

For the Michaelis complex, corresponding to ES in Fig. 3, the optimized structure reveals a pentacoordinated zinc with both the water O_W and the substrate O_P oxygens bound to the metal ion (see Fig. 6). Even though the Zn- O_P distance of 2.18 Å may appear rather short, the interaction between Zn and the substrate via O_P in ES is the weakest one along the entire reaction pathway. At the same time, the Lewis acidity is enhanced towards O_W . This follows from the variations of the distances, where for this structure the water oxygen O_W obtains its closest distance of 2.08 Å to Zn, while the peptide oxygen O_P obtains its most distant one of 2.18 Å. The calculated binding energy of the substrate in the ES structure is quite small, only about 5.8 kcal/mol,

as obtained by removing the substrate to infinite distance. This value can be compared to the binding energy of 2.6–4.6 kcal/mol, corresponding to the observed K_M values for different substrates [6].

The water is strongly acidified with a pK_a going from ~ 14 in the solution phase to ~ 7 or even lower when it is bound to the metal in zinc enzymes, as has been emphasized in many studies [15]. In the ES complex the water molecule is strongly polarized between the negative glutamate, which is a strong base, and the zinc cation (the $O_1-H_1-O_W-Zn$ linkage in Fig. 3). Expansion of the H_1-O_W distance to 1.60 Å from the equilibrium in the ES structure value of 1.09 Å, followed by a

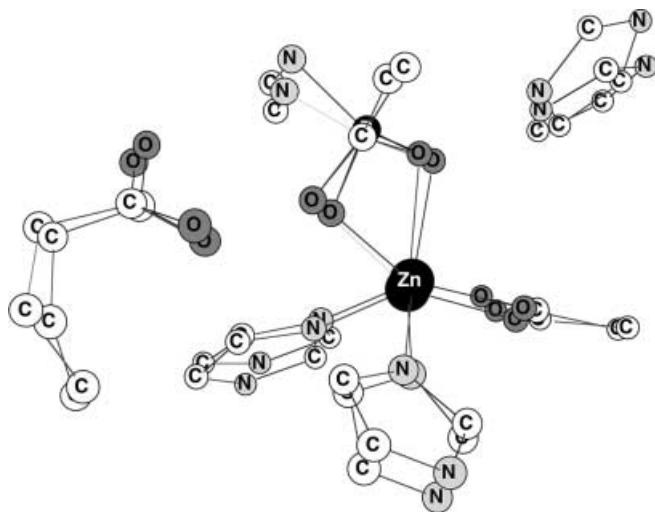


Fig. 5 Active site of TLN inhibited with ZF^pLA phosphoramidate taken from the X-ray structure [27] and merged with the presently optimized INT structure. Only heavy atoms are shown

constrained optimization, leads to an estimated energy cost for the deprotonation of the catalytic water by Glu143 of only 8.9 kcal/mol, compared to an estimated value of 24 kcal/mol for water separation into H^+ and OH^- in a neutral solution [49]. The result is in quite good agreement with the experimental value of 8 kcal/mol for the deprotonation of the Glu143- H_2O -Zn linkage, obtained from the pH and temperature dependence of the enzyme activity [50].

The nucleophilic attack by water on the substrate, going from the ES Michaelis complex to the *gem*-diolate structure INT, is the rate-limiting step for the hydrolysis, with a calculated activation energy of 17.4 kcal/mol for model A. The corresponding transition state TS1 is shown in Fig. 7. This transition state was unusually difficult to determine, partly because a large number of geometrical rearrangements are involved. The most remarkable one is the motion of the carboxylate side chain of Glu143. The superimposed structures of ES and INT in the framework of the frozen edges show a large (~ 1.0 Å) displacement of the carboxyl motif during the proton transfer, with a maximum value of 1.2 Å for O_1 . The water is being deprotonated by Glu143, as was already mentioned above, and the resulting hydroxyl group concertedly approaches the amide carbon C_P . The polarization of the substrate in TS1 is accomplished via the mutual action of two catalytic subunits. First, the Zn atom, which switches the Lewis acidity strength from O_W to O_P , compared to the one in ES. O_P here becomes a very favorable ligand for zinc, approaching the metal ion as close as 2.00 Å, which is the closest Zn-ligand distance observed among all the structures optimized here. The second subunit important for the polarization is the His231 residue, which forms a quite strong hy-

Table 2 Important geometrical parameters of the optimized model A for the intermediate INT compared to the available relevant X-ray and model data. The corresponding geometrical parameters are also given for the other optimized structures along the mechanistic pathway (distances in ångstroms, angles in degrees)

	ES	TS1	INT	4TMN ^a	7TMN ^b	TS2	PROD
Intrapeptide distances							
C_P-N_P	1.35	1.45	1.64	1.90	1.60	2.03	3.77
C_P-O_P	1.28	1.38	1.36	1.58	1.50	1.33	1.31
C_P-O_W	2.89	1.57	1.44	1.59	1.50	1.36	1.30
Zinc-ligand geometry							
$Zn-O_P$	2.18	2.00	2.12	2.17	–	2.14	2.08
$Zn-O_W$	2.08	2.33	2.17	2.59	–	2.21	2.45
$Zn-N_{His142}$	2.10	2.10	2.10	2.09	–	2.09	2.07
$Zn-N_{His146}$	2.18	2.12	2.12	2.11	–	2.11	2.09
$Zn-O_{Glu166}$	2.02	2.01	1.99	2.04	–	2.00	1.98
O_W-Zn-O_{Glu166}	141.11	159.42	156.84	143.99	–	155.44	155.32
O_W-Zn-N_{His142}	107.35	94.04	94.98	93.30	–	96.05	93.70
$N_{His142}-Zn-O_{Glu166}$	111.37	106.48	107.98	121.29	–	108.01	109.87
O_P-Zn-N_{His146}	158.98	135.03	137.31	131.05	–	133.52	130.59
Substrate-enzyme residues selected distances							
O_W-O_2	3.01	2.76	2.45	2.30	–	2.41	2.50
N_P-O_1	3.61	3.22	2.67	3.28	–	2.93	3.06
O_P-N_1	2.88	2.75	2.80	2.70	–	2.80	2.85

^aThe X-ray structure for the enzyme, complexed with the ZF^pLA inhibitor [27], where the C_P carbon in the table notations replaces the phosphoramidate phosphorus

^bThe interactive computer graphics model of the transition state [27]

of the metal towards the substrate [31]. However, the present calculations show that zinc in TLN is in fact capable of holding both OH^- and the substrate during the hydrolysis, partly due to the flexibility of the coordination sphere.

Cleavage of the C-N bond and product formation

The carbon-nitrogen bond of the substrate in the INT *gem*-diolate intermediate is quite ionic, since the $\text{C}_\text{P}\text{-N}_\text{P}$ distance of 1.64 Å is too long to be an ordinary covalent C-N σ -bond (normally about 1.47 Å). Thus, the collapse of the INT structure to the products occurs relatively easy, with a barrier of only 2.9 kcal/mol at the B3LYP/LANL2DZ level. The optimized transition state TS2 is shown in Fig. 8. The Glu143 carboxylate, which in the INT structure is unprotonated, readily accepts the second H_2 proton from O_W to O_2 . The $\text{C}_\text{P}\text{-N}_\text{P}$ bond dissociates heterolytically with an internuclear separation of 2.03 Å at the transition state and the N_P nitrogen retains both electrons.

The final optimized product complex PROD is shown in Fig. 9. This complex has a bidentate bond between zinc and the acetate part of the product of the hydrolysis. Existence of the enzyme-carboxylate complex is in good agreement with structures found in studies of peptide deformylases (PDFs), which are closely related to TLPs (the PDFs transfer a formyl group from one formyl peptide to another via a “ping-pong” mechanism [52]). The methylamine part of the product is only weakly bound to the active site via a single hydrogen bond to the Glu143 O_1 oxygen, with $\text{O}_1\text{-H}_1$ equal to 2.04 Å. This is also in good accordance with kinetic studies on the TLN-catalysed reverse process of peptide bond formation, indicating that the carboxyl-containing substrate binds first, followed by

the amine-containing substrate [26, 53]. As has been suggested by Matthews et al. [26], the second proton transfer by Glu143 towards the N_P nitrogen probably facilitates the formation of the products. In the present model, this is unnecessary for the peptide bond cleavage. However, a protonated amine should fit the pH condition of a neutral solution better. The protonation of the N_P amine nitrogen can instead be considered as the next step of the product conversion, where the H_2 hydrogen, transferred to the Glu143 carboxylate in PROD, probably can be delivered to the amine. Demonstrated to be very flexible in the first H_1 proton shuttling, the Glu143 carboxylate is a strong candidate for this function.

Energetics of the hydrolysis

Single-point calculations using the extended basis set were performed for the two largest models, A and C in Table 1. A diagram of the free energies, including zero-point vibrational effects, entropy contributions and dielectric effects, is shown in Fig. 10. Both models give similar trends. All the values in this subsection refer to the C model, the largest and the most advanced one. A few comments should be made concerning how the energies for this model were obtained. The geometries for this model were not fully optimized but instead the geometries of the His231-Asp226 pair were taken from the fully optimized C' model and merged with the geometries of the A model, which were also fully optimized. Zero-point, entropy and dielectric effects for the C model were also taken from the A model.

The calculated energy of 15.2 kcal/mol for the rate-limiting TS1 step agrees well with TLN standard-state Gibbs activation energies of 12.4–16.3 kcal/mol, derived from k_cat data for different substrates reported to obey

Fig. 8 Optimized transition state TS2 structure for the direct C-N bond cleavage. Atoms marked with an *asterisk* were frozen during the optimization

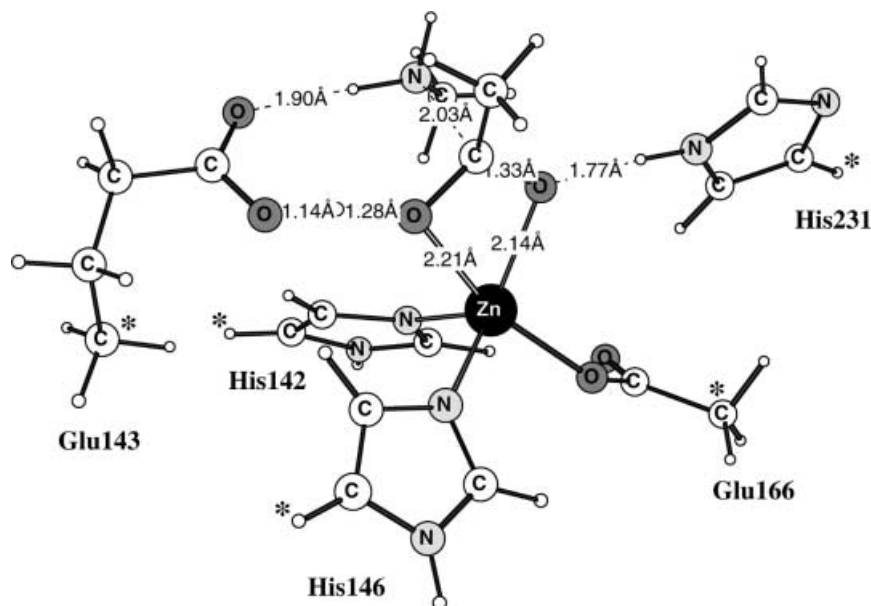


Fig. 9 Optimized PROD structure for the final hydrolysis products. Atoms marked with an *asterisk* were frozen during the optimization

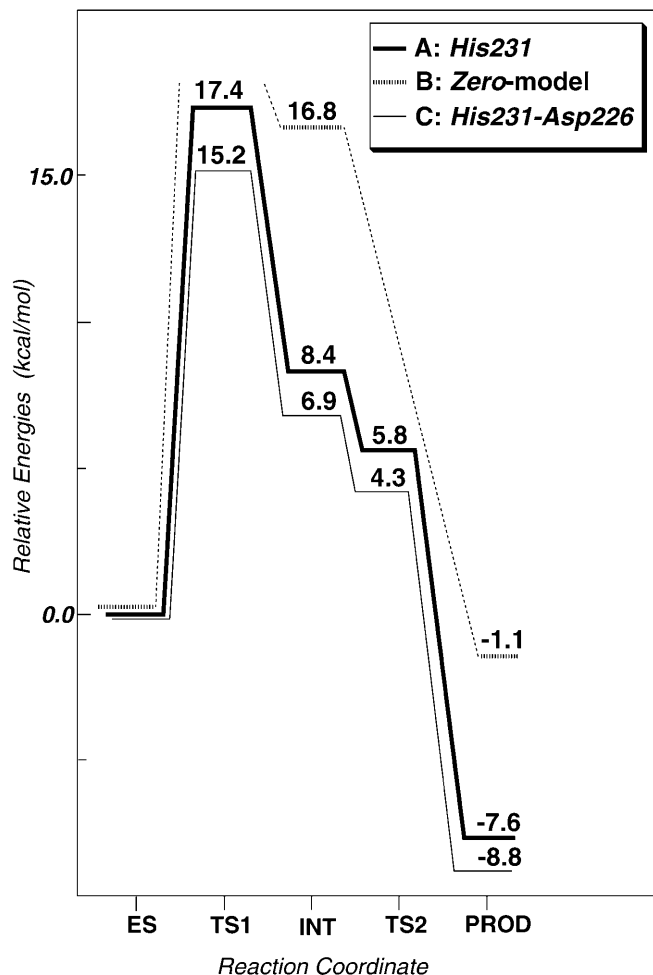
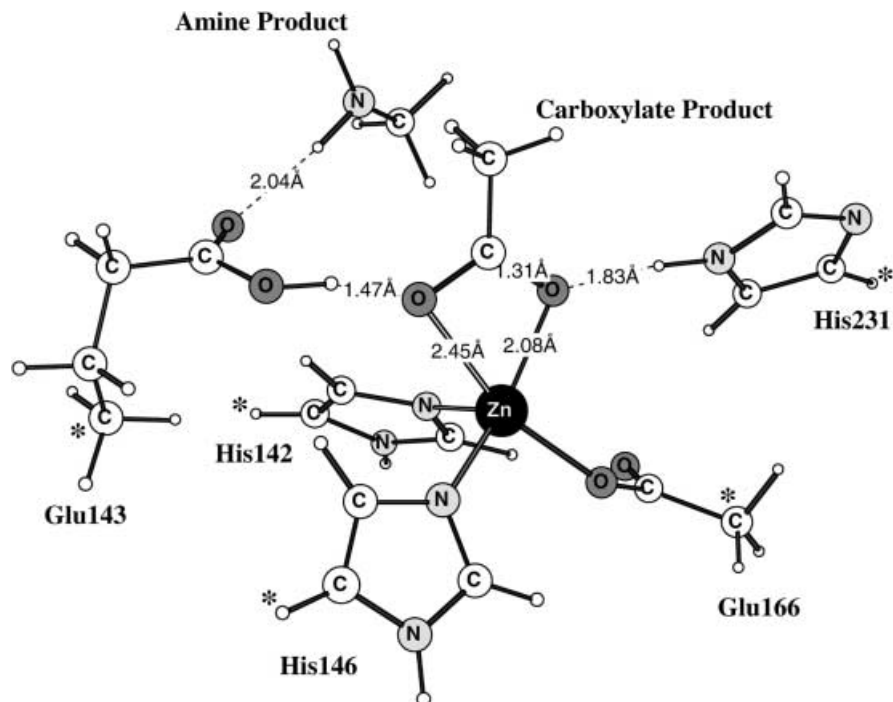


Fig. 10 Potential free energy surface obtained for the A, B and C models

Michaelis-Menten kinetics [6]. Another interesting point is that the accurate energy values place the TS2 energy below the one of the INT structure. This means that, at the highest level used here, there is just a *single step* in the catalytical mechanism for TLN.

It should be added here that the description of the amine product in the present model is not quite satisfactory. The amine moves out a considerable distance, which would not be possible without a cost in the actual enzyme. This means that the exothermicity of 8.8 kcal/mol for the reaction is therefore somewhat too large. We conclude that after the second transition state TS2 our model is probably less valid. After or even during the step of the intermediate collapse, macromolecular phenomena of the product release and reactants uptake can occur, which cannot be described by the model. However, since the main emphasis of the present study is on the mechanism for the actual hydrolysis, this minor problem in the model does not modify any of the conclusions drawn here.

Energetic effect of His231

In the section “Initial enzyme-substrate complex and the nucleophilic attack by water” the importance of the His231 residue in facilitating the activation of the zinc-bound substrate was pointed out. To investigate the importance of His231 further, the imidazole modeling its side chain was eliminated from the A model, leading to the model B of the active site, designated also as the *zero* model. All the other residues and the substrate are the same as in the A model. Using the geometries obtained for the A model as a starting point, analogous stable

minima along the reaction profile (i.e. ES, INT and PROD) were optimized.

The comparison of the potential energy surfaces for the A and B models (see Fig. 10) shows that elimination of His231 leads to a large increase of the relative energy of the INT intermediate by 8.4 kcal/mol. Again, zero-point vibrational effects, entropy contributions and dielectric effects were taken from the A model. The TS1 transition state was not determined for the model without imidazole, but since the product energy of this step is so strongly increased and the hydrogen bonding by H₃ of His231 to the carbonyl oxygen O_P is strongest at the transition state, it is expected that the barrier for the reaction will increase by at least 10 kcal/mol. Clearly, the system is very sensitive to the presence of electrophilic agents in the proximity to the carbonyl oxygen O_P of the activated peptide in the intermediate, since this oxygen is negatively charged. There is actually one more residue which is not included in our models and which is proposed to play a similar role as His231, and this is Tyr157 (see Fig. 1). Together with the zinc cation, these two residues form an “oxyanion hole” [26] in the active site, favorable for the stabilization of the tetrahedral intermediate and for substrate docking. From our results, the docking function may be the more important one for Tyr157, since the A model for TLN has a low enough barrier for hydrolysis even without Tyr157, consistent with a previously suggested only minor role of Tyr157 in stabilizing the transition state [20]. The k_{cat} kinetics data for the independent mutations of His231 and Tyr157 indicate an effect on the activation barrier of 3.4–3.7 kcal/mol for the His231-substituted TLN and a somewhat smaller effect of 2.7 kcal/mol for the Tyr157-substituted enzyme. The K_{m} values suggest Tyr157 to be slightly more important for the substrate binding, with a decreased affinity after mutation of 0.5 kcal/mol, compared to 0.2 kcal/mol for His231 [19, 20] (the same substrate leucine enkephalin was used in the kinetic measurements). Unfortunately, the double His231/Tyr157 mutation for TLN, which would have better corresponded to the results of our B model where both these residues are absent, does not appear to have been made. Thus, the experimental value of 3.4–3.7 kcal/mol for the increase of the activation barrier upon His231 mutation cannot be directly compared with our calculated value of 8.4 kcal/mol, since Tyr157 could partly compensate for the loss of His231 in the real enzyme [20].

Energetic effect of Asp226

The His231 residue, which is demonstrated by the results discussed above to play an important role for hydrolysis, forms a protonated linkage with the Asp226 carboxylate in the enzyme (see Fig. 1). The Asp-His linkage is commonly present in protein structures, and efficiently increases the acidity of the hydrogen bound to the opposite nitrogen of the protonated imidazole ring. To

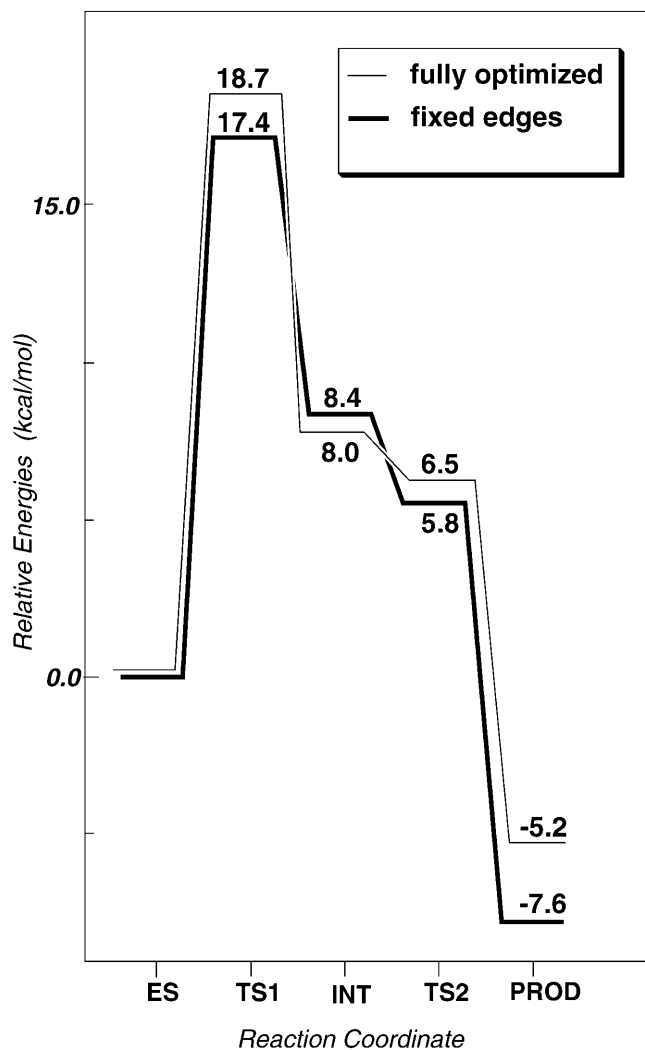


Fig. 11 Potential energy surface obtained for the reaction pathway with and without terminal freezing for the A model

test the importance of Asp226, this residue was included in model C, as already described in the section “Energetics of the hydrolysis”. After geometry optimization of the C’ model, the H₄ proton in between His231 and Asp226 turns out to be actually closer to the carboxylate with H₂-O₃ = 1.1 Å and with N₂-O₃ = 2.6 Å. The Asp226 carboxylate and His231 imidazole ring atoms were found to be in one plane.

Experiments on a TLN mutant where Asp226 was substituted with alanine have been reported to affect the Michaelis-Menten kinetic parameters by an increase of K_{m} , equivalent to the loss of substrate affinity by 1.3 kcal/mol, and a decrease of k_{cat} , equivalent to an increase of the activation barrier by 0.8 kcal/mol [20]. The overall effect of 2.2 kcal/mol was explained as a perturbation of the hydrogen-bonding network in the vicinity of His231, leading to a displacement of this residue and a less efficient stabilization of the transition state. However, the present model results indicate that there is also a *purely electronic* effect of the presence of

the Asp226 at the active site. In Fig. 10 the potential energy surface for the C model is shifted down, compared to A, by 2.2 kcal/mol for the critical TS1 step. As the reaction proceeds, the effect of Asp226 gradually decreases to a 1.1 kcal/mol lowering for the relative energy of the PROD structure. Since the largest effect occurs for the case of TS1, it suggests that the linkage between Asp226 to His231 is primarily important for the transition state stabilization in the reaction mechanism presented.

Optimization without frozen edges

Even with the edges of the system frozen (see beginning of Results and discussion for details), rather large displacements of some residues were observed inside the TLN active site during the catalysis. Since the size of the A model is quite large, it allows for a proper description of these “inner” effects as motions of the Glu143 carboxylate and rotation of the His231 imidazole ring during the first reaction step. The significance of further protein strain in the TLN active site can be estimated through the release of the atoms fixed in the A model followed by a reoptimization of the structures. The geometries and energies obtained via the full optimization show a surprisingly high degree of resemblance to the results for the frozen edges model, and the conceptual hydrolytic pathway as in Fig. 3 remains the same. For the structures, the reactive core and the zinc coordination sphere displays no significant change upon the release of the constraints. The absolute deviation of the Zn-ligand distances, averaged over the five ligands and the five stationary points, is 0.03 Å only, with a maximum value of 0.23 Å. For the coordination angles, the averaged absolute deviation is 3.8°, with a maximum value of 18°. On the other hand, for the outer regions, rather large motions occur. The largest displacement of about 3.6 Å was observed for the edge of the Glu143 side-chain, modeled by the quite bulky butyrate. The energies in Fig. 11 show the rate-limiting TS1 barrier to be slightly higher by 1.3 kcal/mol, compared to the corresponding maximum for the A model with fixed terminals.

The present results suggest that the reactive core in TLN is not very strained by the surrounding enzyme. Therefore the assumption that the protein provides an energized *entatic* [15, 54] state of the metal binding site, significantly distinct from free smaller complexes, is not valid here. The results also suggest that the hydrolytic activity is quite stable against structural perturbations of the protein, which could be an advantage for the enzyme. However, there may still be a minor positive effect of enzyme strain, since the activation energy increases slightly when the terminal atoms are completely free. Concerning the possible hinge-bending motions as mentioned in the beginning of this section, we find no importance for such type of phenomena at the essential catalytic point of the peptide bond cleavage.

Other mechanisms and models

Several other mechanisms for peptide hydrolysis, different from those described above, were examined during this study. None of them seemed to result in a low enough activation barrier, and therefore the investigations performed for these models are much less elaborated. A short summary of the most important results are given below, and it should be noted that the relative energies discussed in this section are calculated at the B3LYP/LANL2DZ level. Terminal freezing, as described at the beginning of “Results and discussion”, has been applied with a few exceptions mentioned below.

In the first set of calculations discussed here, the possibility to decrease the size of the model system by using smaller amino acid models was tested. The imidazole models of the metal histidine ligands His142 and His146 were replaced by simple CH₂-NH imine molecules, analogously to the C' model discussed above. The side-chains of both Glu143 and Glu166 in the A model were described by formates. This model is described in Table 1 as model A'. The formate modeling Glu143 was set completely free during the geometry optimization, since the corresponding carboxylate motif moves significantly during the reaction, as shown in the section “Initial enzyme-substrate complex and the nucleophilic attack by water”. Using this A' model, the relative energy between the enzyme-substrate ES complex and the following INT intermediate was found to be reproduced with sufficient accuracy compared to the larger A model. This result means that mechanistic comparisons performed using this type of smaller amino acid models should be reliable.

Using the B model (see Table 1), an alternative pathway with complete water abstraction to the solvation sphere before the nucleophilic attack was investigated. Such a mechanism has been termed the *zinc-carbonyl* mechanism, and here the role of the metal cation is solely to act as a Lewis acid polarizing the bound substrate, and thereby activating its electrophilic properties [12, 15]. Starting from the pentacoordinated enzyme-substrate ES complex, displacement of the water ligand from zinc leads to a structure with tetrahedral zinc, and with the water molecule hydrogen bonding to the Glu143 carboxylate. It has been shown previously that the release of the first water molecule into the solvation sphere by pentaqua zinc complexes to form a tetrahedral coordination is thermodynamically feasible, generally with a small exothermicity of a few kcal/mol [55, 56]. However, for the present system this type of water loss to the second solvation shell is found to be endothermic by 11.3 kcal/mol. The main reason for this is the presence of the Glu143-H₂O-Zn favorable linkage in the pentacoordinated complex, where the water is positioned between the oppositely charged moieties. While increasing the electrophilic potential of the C_p peptide carbon, the four-coordinated Zn scheme provides less efficient polarization of the abstracted water reactant, and therefore it is not expected that a low

activation energy would result from this type of water displacement mechanism. Moreover, the five-coordinated Zn pathway is strongly supported by extended model investigations [26] based on the X-ray structures of the native and inhibited enzyme. Comparison of the mono- and bidentate coordination to zinc of the *gem*-diolate intermediate shows the latter one to have the most favorable interaction with the active site cleft.

The different A, B and C models, as described above, correspond to different approximations of the His231 influence on the reaction mechanism. Instead of explicit modeling of the His231-Asp226 linkage as in the C and C' models, a protonated His231 could simply be used. In contrast to the systems previously characterized, this model is thus positively charged and is labelled A⁺ in Table 1. The located pentacoordinated complex, similar to the ES structure as discussed above, is only in a very shallow minimum and is unstable in the A⁺ model, where the substrate loses coordination to zinc. The charged imidazolium forms a strong hydrogen bond to the peptide oxygen (O_P-N₁=2.58 Å), creating a very deep minimum of about -13.0 kcal/mol for the enzyme-substrate complex relatively to the INT-like intermediate. The INT-like intermediate and the final PROD-like product structures show only negligible differences to the corresponding minima of the A, B and C models, reproducing the pentacoordinated Zn. The model A⁺ with a protonated histidine thus leads to a deep minimum for the enzyme-substrate complex, with the substrate in a very unfavorable position for the subsequent steps.

The glutamate side-chain is generally accepted to be deprotonated at the neutral pH typical for TLN. However, for a rather modest cost of energy of only a few kcal/mol the carboxylate of the glutamate can be protonated, and it was therefore decided to investigate the effects of using a neutral Glu143 residue in the mechanistic proposal similar to the one described above. Protonating the O₁ oxygen of the Glu143 allows a combination of the nucleophilic water attack and the amino group protonation in a single concerted step, omitting the long-range proton transfer from the water molecule. Such a mechanism also has the advantage that Glu143 is directly reprotonated in the synchronous double-proton transfer. The model used to investigate this aspect is labelled D⁺ since it is positively charged. The protonated Glu143 is modeled by formic acid and the other features of the model are listed in Table 1. In contrast to the generally applied terminal freezing, the D⁺ model was optimized without constraints. The water molecule was placed in the solvation sphere, bound to Glu143 with two hydrogen bonds, thus yielding an enzyme-substrate complex with a tetrahedral Zn. The activation energy obtained for the first step is 17.6 kcal/mol, and the following *gem*-diolate intermediate is 6.8 kcal/mol, relative to the initial enzyme-substrate complex. This reaction proceeds with a four-coordinated zinc, satisfying the zinc-carbonyl pathway, as discussed above. It turns out that within the D⁺ model the second step of the C_P-N_P bond cleavage is the main problem,

with a barrier several tens of kcal/mol higher than for the first step, completely ruling out this type of mechanism. One possible explanation for the high activation energy for the C-N bond cleavage is that the product of this step is severely destabilized compared to the main neutral model. Such a destabilization could arise from a weaker interaction between the coordinated neutral carboxylic acid product and the positively charged zinc, compared to the negatively charged carboxylate product and a positive zinc obtained in the overall neutral model (compared to the generally studied mechanism, the O₂ oxygen of the Glu143 carboxylate is already reprotonated in the intermediate of the D⁺ model, and no suitable proton acceptor from the Zn-bound product is therefore available). Another explanation for the high activation energy could be an increased cost to move the amine product away from the overall positively charged zinc center compared to the main model with an overall neutral zinc center.

Finally, in line with a previous suggestion for the hydrolysis by TLN [32], a few calculations were performed to investigate the effect of including a second water molecule in the hydrolysis. In this case the extended models for the substrate and Glu143 together with the simplest models for the structural ligands of Zn were used (see model E in Table 1). The His231 residue was not included. The reaction starts from the ES-like enzyme-substrate structure with the favorable Glu143-H₂O-Zn linkage, and the second water molecule coordinated by the O₁ oxygen of the Glu143. In the first step the proton transfer occurs via the water molecule chain, thus leaving only a coordinating role for the Glu143. Qualitatively, the resulting *gem*-diolate intermediate differs from the INT structure obtained with the A model as shown in Fig. 4 only by the additional water molecule inserted between the Glu143 O₁ oxygen and the H₁ hydrogen, thus replacing the O₁-H₁ hydrogen bond (the labels used are as in Fig. 3). However, the relative energy for this intermediate is found to be significantly higher in the two-water model, even considering possible effects from including His231. Therefore, the preliminary results predict that a second water molecule introduced in this way would have a rather negative effect on the first catalytic step, making it too slow. The additional water molecule forces the negatively charged Glu143 carboxylate motif further away from the positively charged amine end of the substrate in the intermediate, introducing a larger charge separation, which could explain the energy increase.

Conclusions

The mechanism of peptide hydrolysis by thermolysin-like Zn²⁺-metalloproteases (TLPs) has been investigated using the B3LYP hybrid DFT method. The starting structure was based on the X-ray crystallographic data [27] for the enzyme complexed with the phosphoramidate ZF^pLA inhibitor. In line with

previous biochemical proposals [27, 28], ZF^PLA was found to be a relevant transition state analogue. The ZF^PLA-inhibited active site closely matches the optimized structure of the metastable intermediate labelled INT (see Fig. 4 and Fig. 5), which corresponds to the midpoint of the catalytic path in the present study.

The mechanism presented here is essentially a *single-step* reaction, schematically shown in Fig. 3 and with a free energy profile as shown in Fig. 10. The transition state for the nucleophilic water attack on the peptide carbon, TS1 (Fig. 7), was found to have an activation energy of 15.2 kcal/mol, which fits well to the experimental results in the range 12.4–16.3 kcal/mol. After the formation of the enzyme-substrate complex ES (Fig. 6), the zinc cofactor remains pentacoordinated along the entire reaction owing to the flexibility of the coordination sphere. Therefore, the mechanism presented has elements from both the *zinc-carbonyl* and the *zinc-hydroxide* mechanisms proposed in the early days of the zinc metalloenzymes studies (while the first concept proposes the incoming substrate to bind directly to Zn and completely displace the metal-bound water, the second one proposes zinc to mediate its function through the catalytic water molecule, with no direct coordination of the substrate to Zn).

Among the active site residues, Glu143 is confirmed to play a key role, abstracting a proton from the metal-bound water and shuttling this proton to the peptide nitrogen. In the final part of the mechanism, the Glu143 carboxylate accepts the second proton, facilitating the formation of the experimentally postulated enzyme-carboxylate complex, which corresponds to the final products, PROD (Fig. 9), in the present study. The presence of additional electrophilic agents in the proximity of the Zn-bound carbonyl oxygen of the substrate significantly favors the enzymatic efficiency. Inclusion of the neighboring His231 in its neutral form provides a stabilization effect of 8.4 kcal/mol for the *gem*-diolate intermediate INT (A versus B models). The proper modeling of the His231-Asp226 protonated linkage (C model) allows a further decrease of the activation energy by 2.2 kcal/mol, in line with experimental observations for Asp226-mutated TLN kinetic studies.

The two extreme cases for treating strain from the surrounding protein, without constraints and with fixed side-chain edges, respectively, examined for the A model display only small differences. Both the reactive core geometries and the energy surfaces (Fig. 11) are essentially the same. There is only a slight decrease of the activation energy by 1.3 kcal/mol for the frozen edge model. Still, the positioning of the chemical units seems to be exceptionally optimized by the enzyme to promote the catalytic action.

References

- Lipscomb WN, Strater N (1996) *Chem Rev* 96:2375–2433
- Blundell TL (1994) *Nat Struct Biol* 1:73–75
- Roques BP (1993) *Biochem Soc Trans* 21:678–685
- Endo S (1962) *J Ferment Technol* 40:346
- Matsubara H, Sasaki R, Singer A, Jukes TH (1966) *Arch Biochem Biophys* 115:324–331
- Morihara K, Tsuzuki H (1970) *Eur J Biochem* 15:374
- Eichhorn U, Bommarius AS, Drauz K, Jakubke H-D (1995) In: Maia HLS (ed) *Peptides 1994*. Escom, Leiden, pp 226–227
- Rao MB, Tanksale AM, Ghatge MS, Deshpande VV (1998) *Microbiology* 62:597–635
- Matthews BW, Jansonius JN, Colman PM, Schoenborn BP, Dupourque D (1972) *Nature* 238:37
- Matthews BW, Colman PM, Jansonius JN, Titani K, Walsh KA, Neurath H (1972) *Nature* 238:41
- Colman PM, Jansonius JN, Matthews BW (1972) *J Mol Biol* 70:701
- Vallee BL, Auld DS (1990) *Proc Natl Acad Sci USA* 87:220–224
- Rulišek L, Vondrášek JJ (1998) *Inorg Biochem* 71:115–127
- Alberts JL, Nadassy K, Wodak SJ (1998) *Protein Sci* 7:1700–1716
- Galdes A, Vallee BL (1983) In: Siegel H (ed) *Metal ions in biological systems*, vol 15. Dekker, New York, pp 6–7
- Holland DR, Hausrath AC, Juers D, Matthews BW (1995) *Protein Sci* 4:1955–1965
- Toma S, Campagnoli S, De Gregoris E, Gianna R, Margarit R, Zamai M, Grandi G (1989) *Protein Eng* 2:359–364
- Kubo M, Mitsuda Y, Takagi M, Imanaka T (1992) *Appl Environ Microbiol* 58:3779–3783
- Beaumont A, O'Donohue MJ, Paredes N, Rousselet N, Assicot M, Bohuon C, Fournié-Zaluski M-C, Roques BP (1995) *J Biol Chem* 270:16803–16808
- Marie-Claire C, Ruffet E, Tiraboschi G, Fournié-Zaluski M-C (1998) *FEBS Lett* 438:215–219
- Marie-Claire C, Ruffet E, Antonczak S, Beaumont A, O'Donohue M, Roques BP, Fournié-Zaluski M-C (1997) *Biochemistry* 36:13938–13945
- Veltman OR, Eijssink VGH, Vriend G, De Kreijl A, Venema G, Van den Burg B (1998) *Biochemistry* 37:5305–5311
- Pangburn MK, Walsh KA (1975) *Biochemistry* 14:4050–4054
- Kester WR, Matthews BM (1977) *Biochemistry* 16:2506–2516
- Holmes MA, Matthews BW (1981) *Biochemistry* 20:6912–6920
- Hangauer DG, Monzingo AF, Matthews BW (1984) *Biochemistry* 23:5730–5741
- Holden HM, Tronrud DE, Monzingo AF, Weaver LH, Matthews BW (1987) *Biochemistry* 26:8542–8553
- Matthews BW (1988) *Acc Chem Res* 21:333–340
- Bartlett PA, Marlowe CK (1987) *Biochemistry* 26:8553–8561
- Mock WL, Aksamavati M (1994) *Biochem J* 302:57
- Mock WL, Stanford DJ (1996) *Biochemistry* 35:7369
- Antonczak S, Monard G, Ruiz-Lopez MF, Rivail J-L (1998) *J Am Chem Soc* 120:8825–8833
- Antonczak S, Monard G, Ruiz-Lopez MF, Rivail J-L (2000) *J Mol Model* 6:527–538
- Becke AD (1988) *Phys Rev A* 38:3098
- Becke AD (1993) *J Chem Phys* 98:1372
- Becke AD (1993) *J Chem Phys* 98:5648
- Frisch MJ, Trucks GW, Schlegel HB, Gill PMW, Johnson BG, Robb MA, Cheeseman JR, Keith T, Petersson GA, Montgomery JA, Raghavachari K, Al-Laham MA, Zakrzewski VG, Ortiz JV, Foresman JB, Cioslowski J, Stefanov BB, Nanayakkara A, Challacombe M, Peng CY, Ayala PY, Chen W, Wong MW, Andres JL, Replogle ES, Gomperts R, Martin RL, Fox DJ, Binkley JS, Defrees DJ, Baker J, Stewart JP, Head-Gordon M, Gonzalez C, Pople JA (1995) *Gaussian 94*, revision B.2. Gaussian, Pittsburgh
- Hay PJ, Wadt WR (1988) *J Chem Phys* 82:299
- Dunning J, Hay PJ (1976) In: Schaefer HF III (ed) *Modern theoretical chemistry*, vol 3. Plenum, New York, p 1
- Gonzales C, Schlegel HB (1990) *J Phys Chem* 94:5523
- Beapak MJ, Robb MA, Schlegel HB (1994) *Chem Phys Lett* 223:269

42. McQuarrie DA (1973) *Statistical thermodynamics*. Harper and Row, New York
43. Wiberg KB, Rablen PR, Rush DJ, Keith TA (1995) *J Am Chem Soc* 117:4261
44. Wiberg KB, Keith TA, Frisch MJ, Murcko M (1995) *J Phys Chem* 99:9072
45. Siegbahn PEM, Blomberg MRA (2000) *Chem Rev* 100:421–437
46. Kudryashova EV, Mozhaev VV, Balny C (1998) *Biochim Biophys Acta* 1386:199–210
47. Warshel A (1981) *Acc Chem Res* 14:284
48. Holland DR, Tronrud DE, Pley HW, Flaherty KM, Stark W, Jansonius JN, McKay DB, Matthews BW (1992) *Biochemistry* 21:11310
49. Siegbahn PEM (1996) *J Comput Chem* 17:1099–1107
50. Kunugi S, Hirohara H, Ise N (1982) *Eur J Biochem* 124:157–163
51. Prabhakar R, Blomberg MRA, Siegbahn PEM (2000) *Theor Chem Acc* 104:461–470
52. Becker A, Schlichting I, Kabsch W, Groche D, Schultz S, Wagner AFV (1998) *Nat Struct Biol* 5:1053–1058
53. Oyama K, Kihara K, Nonaka Y (1981) *J Chem Soc Perkin Trans 2*: 356
54. Williams RJP (1995) *Eur J Biochem* 234:363–381
55. Pavlov M, Siegbahn PEM, Sandström M (1998) *J Phys Chem A* 102:219
56. Hartmann M, Clark T, van Eldik R (1996) *J Mol Model* 2:354–357